Demonstration of a Quantum Switch in a Sagnac Configuration

Teodor Strömberg,[1,2,*] Peter Schiansky,[1,2] Robert W. Peterson,[2] Marco Túlio Quintino,[3,4,5] and Philip Walther[2,†]
[1]University of Vienna, Faculty of Physics & Vienna Doctoral School in Physics, Boltzmanngasse 5, A-1090 Vienna, Austria
[2]University of Vienna, Faculty of Physics & Research Network Quantum Aspects of Space Time (TURIS), Boltzmanngasse 5, 1090 Vienna, Austria
[3]Sorbonne Université, CNRS, LIP6, F-75005 Paris, France
[4]University of Vienna, Faculty of Physics, Boltzmanngasse 5, 1090 Vienna, Austria
[5]Institute for Quantum Optics and Quantum Information, Boltzmanngasse 3, 1090 Vienna, Austria

(Received 24 November 2022; accepted 12 July 2023; published 11 August 2023)

The quantum switch is an example of a process with an indefinite causal structure, and has attracted attention for its ability to outperform causally ordered computations within the quantum circuit model. To date, realizations of the quantum switch have made a trade-off between relying on optical interferometers susceptible to minute path length fluctuations and limitations on the range and fidelity of the implementable channels, thereby complicating their design, limiting their performance, and posing an obstacle to extending the quantum switch to multiple parties. In this Letter, we overcome these limitations by demonstrating an intrinsically stable quantum switch utilizing a common-path geometry facilitated by a novel reciprocal and universal SU(2) polarization gadget. We certify our design by successfully performing a channel discrimination task with near unity success probability.

DOI: 10.1103/PhysRevLett.131.060803

Introduction.—Quantum information processing tasks are most commonly described within the framework of the quantum circuit model. In this framework an initial state gradually evolves by passing through a fixed sequence of gates. This, however, is not the most general model of computation that quantum mechanics admits, and in [1] a processes that effects a superposition of quantum circuits was proposed. This process, known as the quantum switch, has attracted significant theoretical [2–5] and experimental [6–13] interest. Together with the so-called Oreshkov-Costa-Brukner process [14] it was the first example of a quantum process without a definite causal structure, and motivated the study of more general causal structures within quantum mechanics that could help bridge the gap between general relativity and quantum mechanics. The quantum switch is also of practical interest, since it has been shown to allow for a computational advantage over standard quantum circuits [15,16], an advantage which has been demonstrated experimentally [17].

In its simplest form, the quantum switch is a map that acts on two gates, U and V, and transforms them into a controlled superposition of the gates being applied in two different orders:

$$(U, V) \mapsto UV \otimes |0\rangle\langle 0|_C + VU \otimes |1\rangle\langle 1|_C. \quad (1)$$

To date, all experimental realizations of the quantum switch have been done using single photons as the physical system encoding the input and output state of the process. These implementations typically rely on folded Mach-Zehnder interferometers (MZIs) and polarization optics to couple different internal degrees of freedom of the single photons. A technical challenge associated with such implementations is that the phase of the interferometer needs to be kept constant even as different choices of U and V in (1) change the interference condition. In practice, most experimental quantum switches have relied on passive phase stability during operation, limiting not only their fidelity, but also their duty cycle due to the need to periodically reset the phase. Furthermore, the geometry of the MZI means that single photons in the two different arms of the interferometer interact with different parts of the polarization optics [see Fig. 1(a)]. The reliance on optical geometries that suffer from phase instability is necessitated by the nonreciprocity of the optical components that effect the unitary transformations U and V on the photon polarization. The works [8,10] remedied this by using the polarization as a control degree of freedom (d.o.f.), instead of a target, thereby enabling a common-path geometry; however, this came at

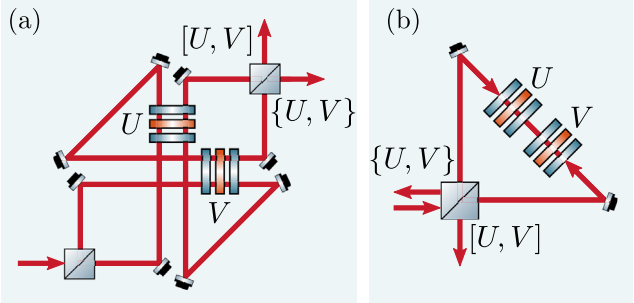

FIG. 1. Path-polarization quantum switch. (a) The most common implementation of the photonic quantum switch utilizes the path degree of freedom of a single photon inside a Mach-Zehnder interferometer to coherently control the order in which two polarization operations U and V are applied. In this geometry, photons in different arms of the interferometer propagate through different parts of the polarization optics. (b) An implementation based on a Sagnac interferometer is fundamentally simpler and more robust, but necessitates two different propagation directions through the polarization gadgets effecting the transformations U and V. In general, the operations in the two different propagation directions are not the same, limiting the use of this geometry to special cases.

the expense of more cumbersome and low fidelity target qubit operations.

In [17] a common-path geometry was realized in a different way, by encoding the target system in the temporal degree of freedom. This implementation, however, was limited to generalized versions of the Pauli X and Z operators, and could therefore not prepare superposition states. These operations furthermore required both ultrafast phase modulators and the manual replacement of optical components, increasing the experimental requirements while reducing the programmability of the setup.

In this Letter, we overcome these limitations by designing a fully reciprocal polarization gadget capable of realizing any $U \in \mathrm{SU}(2)$, thereby enabling the use of a passively stable Sagnac geometry with perfect spatial mode overlap, while still using the polarization d.o.f. for the target qubit, without imposing any restrictions on the unitaries applied on this system inside the quantum switch.

Photonic quantum switch.—In the commonly used path-polarization quantum switch, shown in Fig. 1(a), the path d.o.f. is used to coherently superpose two different orders through the wave plate gadgets that act on the target (polarization) qubit. These wave plate gadgets, first introduced by Simon and Mukunda, consist of two quarter-wave plates and one half-wave plate, and are universal for SU(2) [18]. If one tries to use a common path geometry, as depicted in Fig. 1(b), the photon now travels through the polarization gadgets in two different directions. The action of a Simon-Mukunda gadget in the backwards direction is $U^{\mathrm{bw}} = PU^T P^\dagger \neq U$, where U is the unitary operation in the forwards direction, and P is a unitary operator describing the basis change to the backwards propagation direction. By picking a convention for the polarization states in which the diagonal polarizations are associated with the eigenstates of the Pauli Y matrix one finds that $P = \mathbb{1}$ [19], however, the residual transpose, a consequence of the fact that the order of the wave plates is transposed in the backwards direction, cannot be undone this way. The Simon-Mukunda gadget is therefore only reciprocal for a two parameter subset of SU(2), and common-path quantum switches such as [20], were thus far not able to implement arbitrary polarization unitaries.

In this Letter, we adopt the convention $(S_1, S_2, S_3) \leftrightarrow (X, Y, Z)$ for the Stokes parameters and Pauli matrices. Written in this convention, the Simon-Mukunda gadget transforms as $U \mapsto U^{\mathrm{bw}} = ZU^T Z$ under counterpropagation. Given a unitary parametrized as $U = \exp[-i(\theta/2)\vec{\sigma}\cdot\vec{n}]$, where $\vec{\sigma}$ is the Pauli vector and $\vec{n}$ the rotation axis of the unitary operation on the Bloch sphere, this transformation corresponds to $[\theta, n_x, n_y, n_z] \mapsto [\theta, -n_x, n_y, n_z]$. Since this transformation applies to any unitary operation implemented by a sequence of linear retarders under counterpropagation, we also consider circular retarders, more specifically Faraday rotators. It is a well known fact that Faraday rotators are nonreciprocal, due to the magneto-optic effect breaking Lorentz reciprocity [21]. This property has enabled a multitude of widely adopted optical devices such as Faraday mirrors [22], optical circulators, and optical isolators [23]. Quantitatively, the nonreciprocity manifests itself as the following transformation under counterpropagation $[\theta, n_y] \mapsto [-\theta, n_y]$.

Faraday rotators are usually sold with a fixed circular retardance of $\theta = (\pi/2)$, corresponding to a rotation of linear polarization by 45°. We will therefore restrict our discussion to only these devices, and show how they can be used to construct a fully reciprocal polarization device.

A reciprocal polarization gadget.—Since only the X component of the Simon-Mukunda gadget exhibits nonreciprocity, we begin by constructing a gadget capable of realizing a reciprocal X rotation:

$$G_x(\theta) = H\left(\frac{\pi}{8}\right) F_- Q\left(\frac{\pi}{2}\right) H\left(\frac{\theta + 2\pi}{4}\right) Q\left(\frac{\pi}{2}\right) F_+ H\left(\frac{\pi}{8}\right). \tag{2}$$

Here H and Q refer to half- and quarter-wave plates at a given angle from the vertical axis, and $F_\pm$ are Faraday rotators with circular retardance of $\pm(\pi/2)$. The three middle wave plates constitute a Simon-Mukunda gadget implementing a nonreciprocal X rotation:

$$R_x(\theta + 2\pi) = -R_x(\theta) \mapsto -R_x(-\theta). \tag{3}$$

The action of the G_x gadget in the two different propagation directions can therefore be expressed as

$$G_x^{\mathrm{fw}}(\theta) = -H\left(\frac{\pi}{8}\right) F_- R_x(\theta) F_+ H\left(\frac{\pi}{8}\right) \tag{4}$$

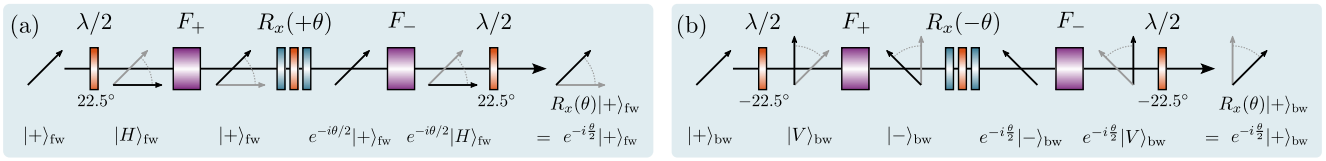

FIG. 2. Reciprocal polarization gadget. The evolution of a diagonally polarized state in the two different propagation directions through a reciprocal R_x gadget. The arrows indicating the polarization states are drawn in the comoving frame. Note that only differential phases between the two polarization components are indicated. (a) The Faraday rotators $F_\pm$ rotate linear polarization by 45°, and in the forwards direction these rotations cancel the half-wave plate (HWP) rotations, indicated by $\lambda/2$. The state before the central wave plate gadget is therefore $|+\rangle$, and the correct phase gets applied. (b) In the backwards propagation direction the rotations of the HWP and Faraday rotators add, rotating the linear polarization by 90°. The $R_x(-\theta)$ rotation applies the desired phase to what is now the $|-\rangle$ state, which subsequently gets rotated back to $|+\rangle$, yielding the correct transformation.

$$G_x^{\mathrm{bw}}(\theta) = -H\left(-\frac{\pi}{8}\right)F_- R_x(-\theta)F_+ H\left(-\frac{\pi}{8}\right), \tag{5}$$

since for a single linear retarder at an angle φ to the vertical axis the effect of reversing the propagation direction is $\varphi \mapsto -\varphi$. The superscripts fw and bw refer to the forwards and backwards propagation directions, respectively. To see that the full gadget is reciprocal, note that

$$H\left(\frac{\pi}{8}\right)F_- = F_+ H\left(\frac{\pi}{8}\right) = -iX, \tag{6}$$

$$H\left(-\frac{\pi}{8}\right)F_- = F_+ H\left(-\frac{\pi}{8}\right) = -iZ, \tag{7}$$

as shown in the Supplemental Material [24]. The action of the gadget in the two propagation directions can therefore be simplified to

$$G_x^{\mathrm{fw}}(\theta) = XR_x(\theta)X = R_x(\theta), \tag{8}$$

$$G_x^{\mathrm{bw}}(\theta) = ZR_x(-\theta)Z = R_x(\theta). \tag{9}$$

A graphical examination of the reciprocity of the gadget is shown in Fig. 2. Using this gadget as a building block, it becomes possible to construct a fully reciprocal gadget capable of implementing arbitrary unitaries:

$$G_R = Q(\theta)H(\phi)G_x(\gamma)H(-\phi)Q(-\theta). \tag{10}$$

This gadget is reciprocal due to its palindromic order, and a proof of its universality, as well as a method to find the angles θ, ϕ, and γ for a given U, is provided in the Supplemental Material [24]. An implementation of this algorithm is available in an open repository [25].

Advantage in a channel discrimination task.—To certify that our experimental platform is capable of realizing an indefinite causal order, we now present a channel discrimination task for which the quantum switch strictly outperforms any causally ordered strategy. This channel discrimination problem was originally presented as a causal witness in Ref. [15] and was inspired by the task introduced in Ref. [3]. Let U_i, V_j be two qubit unitary operators belonging to the set

$$\mathcal{G} \coloneqq \left\{\mathbb{1}, X, Y, Z, \frac{X \pm Y}{\sqrt{2}}, \frac{X \pm Z}{\sqrt{2}}, \frac{Y \pm Z}{\sqrt{2}}\right\}. \tag{11}$$

Using this set, we define two sets of pairs of operators (U_i, V_j) that either commute or anticommute:

$$\mathcal{G}_\pm \coloneqq \{(U_i, V_j) | U_i, V_j \in \mathcal{G}, U_i V_j = \pm V_j U_i\}. \tag{12}$$

Let (U_i, V_j) be a pair of channels belonging to either $\mathcal{G}_+$ or $\mathcal{G}_-$, and consider the task of deciding to which set they belong, given only a single use of the channels. It is well known that this task can be performed deterministically when given access to the quantum switch. This can be seen by setting the state of the control qubit in (1) to $|+\rangle_C$ and considering the action on any target state $|\Psi\rangle_T$:

$$\begin{aligned}&(UV \otimes |0\rangle\langle 0| + VU \otimes |1\rangle\langle 1|)|\Psi\rangle_T \otimes |+\rangle_C \\ &= \frac{1}{2}(UV + VU)|\Psi\rangle_T \otimes |+\rangle_C + \frac{1}{2}(UV - VU)|\Psi\rangle_T \otimes |-\rangle_C.\end{aligned} \tag{13}$$

A measurement of the control qubit then reveals to which set (U_i, V_j) belongs.

For this discrimination task, the probability of successfully guessing the set can be expressed as

$$p_s(i,j) \coloneqq p[\pm|(U_i, V_j)], \quad \text{if } (U_i, V_j) \in \mathcal{G}_\pm. \tag{14}$$

By making use of the semidefinite programming methods presented in Ref. [26], we find that any causally ordered strategy necessarily obeys $\min[p_s(i,j)] \leq 0.841$. Moreover, if the pairs of channels (U_i, U_j) are uniformly picked from $\mathcal{G}_+$ and $\mathcal{G}_-$, the average probability of correctly guessing the set with a causally ordered strategy is bounded by $(1/N)\sum_{i,j} p_s(i,j) \leq 0.904$ where the indices i, j run over all the pairs of gates that commute or anticommute. As discussed in Ref. [15], this average success probability

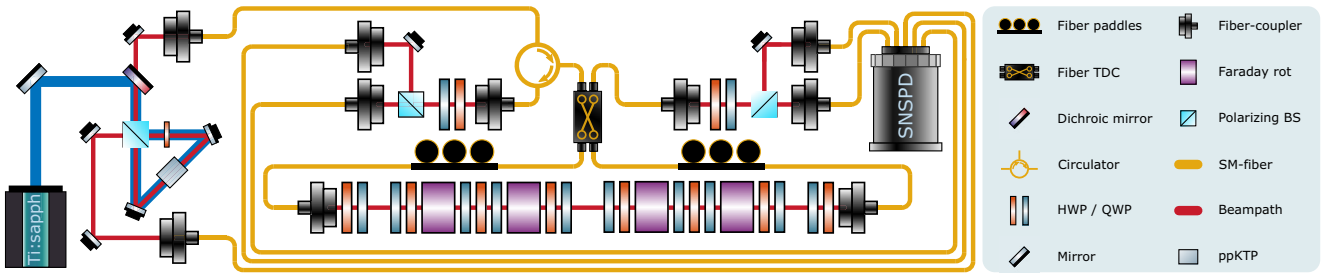

FIG. 3. Experimental setup. Single photons are generated by a type-II spontaneous parametric down-conversion source using a ppKTP crystal. Detection of the signal photon using superconducting nanowire single-photon detectors (SNSPDs) heralds the presence of the idler photon. A tunable directional coupler (TDC) configured for a balanced splitting ratio sends the idler photon through a free-space path in a superposition of two propagation directions. This path contains two reciprocal polarization gadgets consisting of Faraday rotators, quarter-wave plates (QWPs) and half-wave plates (HWPs). These gadgets implement the operators U and V. The photon finally exits in one of the two TDC ports depending on whether U and V commute or anticommute, and is then detected using a polarization resolving measurement. A fiber circulator is used to pick off photons exiting the Sagnac in the input port.

approach can be phrased in terms of a causal nonseparability witness, and in the Supplemental Material [24] we explicitly present such a witness.

Experiment.—Before experimentally performing the channel discrimination task, we first show that the gadget in (10) is indeed reciprocal and universal. To this end we perform quantum process tomography on both gadgets used in the experiment for 100 random unitaries. The resulting gate fidelities, defined as the average state fidelity under the reconstructed unitaries, are presented in the Supplemental Material [24]. Achieving an average gate fidelity of 0.9970 ± 0.0018, and an average fidelity between the two propagation directions of 0.9972 ± 0.0018, we conclude that the gadget is reciprocal and universal.

We now turn to the experimental realization of the quantum switch, pictured in Fig. 3. For the certification of the indefinite causal structure of the implemented process, we employ single photons generated using type-II spontaneous parametric down-conversion [27]. The signal photon is used as a herald for the idler photon, which is made to propagate through the quantum switch. Initially, a beam splitter in the form of a tunable directional coupler (TDC) applies a Hadamard operation on the path (control) d.o.f., thereby preparing the state: $|\Psi\rangle_T \otimes (|0\rangle_C + |1\rangle_C)/\sqrt{2}$, where the subscripts C and T refer to the control and target degrees of freedom, respectively. The photon then passes through the polarization gadgets in a superposition of the two propagation directions, correlating the applied gate order with the control d.o.f.: $(1/\sqrt{2})UV|\Psi\rangle_T \otimes |0\rangle_C + (1/\sqrt{2})VU|\Psi\rangle_T \otimes |1\rangle_C$. Finally, the photon propagates back to the TDC which once again applies a Hadamard gate on the control qubit:

$$\frac{1}{2}\{U,V\}|\Psi\rangle_T \otimes |0\rangle_C + \frac{1}{2}[U,V]|\Psi\rangle_T \otimes |1\rangle_C. \qquad (15)$$

Measuring the photon's location then reveals, with unity probability, whether the gates (U,V) commute or anticommute.

Our implementation makes use of a combination of free-space and fiber optics, which is facilitated by the intrinsic phase stability of the common-path geometry. The use of a fiber TDC allows for precise control over the splitting ratio as well as providing perfect spatial mode overlap. These two factors combine to yield a high interferometric visibility in excess of 0.9995. The two inner ports of the TDC are connected to fiber collimators that launch the photons into free space where they propagate through the two polarization gadgets in opposite directions.

A fiber circulator is placed at the input port of the TDC to separate the backwards propagating photons from the input light. Finally, two measurement stations are used to measure the polarization of the photons in either output arm of the Sagnac. The polarization resolving measurements allow for the polarization dependent detection efficiencies in the superconducting nanowire single-photon detectors used in the experiment to be corrected for. The fiber circulator induces a small amount of differential loss in the two interferometer outputs which is also corrected for (see Supplemental Material [24]).

Results.—Each of the 52 pairs of (anti)commuting unitary operators in the sets (12) were implemented six independent times, and for each pair of operations single-photon events were recorded for 60 sec, giving a total measurement time of approximately 5 h, with the only downtime being the time spent rotating the wave plates. The success probabilities were then calculated separately for each run. The results of this are shown in Fig. 4. We find a minimum success probability of $\min[p_s(i,j)] = 0.9895$, and an average success probability of $\langle p_s \rangle = 0.99639 \pm 0.00007$, far exceeding the causally separable bounds of 0.841 and 0.904, respectively. Our observed average success probability can be directly compared with a non-common-path implementation of an analogous channel discrimination task presented in [6], where a success probability of 0.973 was achieved. The observed success probabilities $p_s(i,j)$ for the individual pairs of gates

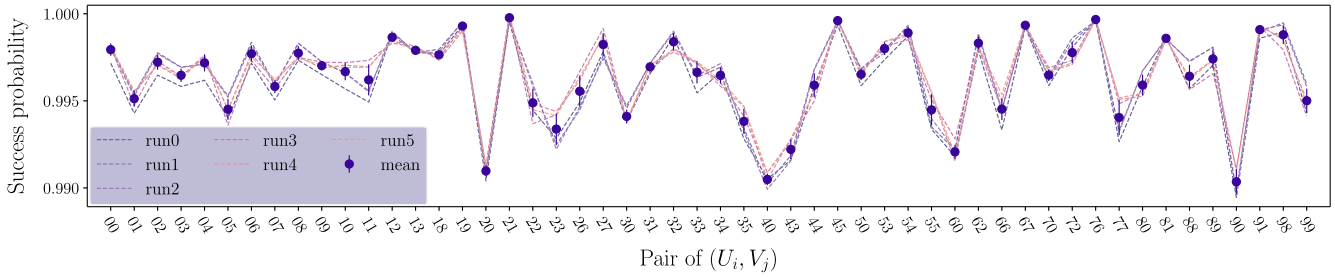

FIG. 4. Success probabilities $p_s(i,j)$ that correspond to the probability for the photon to exit in the correct port of the interferometer given a pair of commuting or anticommuting unitaries (U_i, V_j). The six different runs of the experiment, plotted separately, exhibit high repeatability. Dashed lines show these six different experimental runs, while the solid dots indicate the mean and standard deviation of the runs. The average success probability is $\langle p_s \rangle = 0.9964$, while the highest and lowest success probabilities are $\max[p_s(i,j)] = 0.99997$ and $\min[p_s(i,j)] = 0.9895$, respectively.

(U_i, V_j) additionally display a remarkably low variance, with a recorded standard deviation of $\sigma^2 = 0.0024$, demonstrating the robustness of our design. The uncertainty in the experimentally evaluated success probability is the error-propagated observed standard deviation for the constituent success probabilities $p_s(i,j)$ in the six runs.

Discussion.—We have demonstrated for the first time a path-polarization quantum switch that utilizes a passively stable common-path geometry. Our novel design greatly simplifies the construction and operation of the device, while simultaneously increasing its fidelity, robustness and duty cycle compared to previous demonstrations. The implementation is facilitated by a new polarization gadget that combines different forms of nonreciprocity to unlock fully reciprocal and universal polarization transformations. The methods used to engineer the reciprocity of the polarization gadgets can be applied more broadly to map balanced interferometers onto common-path geometries. This will enable simple and robust bulk-optics realizations of important primitives such as reconfigurable beam splitters and variable partially polarizing beam splitters [28]. We anticipate that this will lead to straightforward realizations of generalized measurements directly on polarization qubits [29], as well as the demonstration of multiparty quantum switches [16].

All data used in this work is openly available at [30].

R. W. P. acknowledges support from the ESQ Discovery program (Erwin Schrödinger Center for Quantum Science and Technology), hosted by the Austrian Academy of Sciences (ÖAW). P. W. acknowledges support from the research platform TURIS, the European Commission through EPIQUS (No. 899368) and AppQInfo (No. 956071), from the Austrian Science Fund (FWF) through BeyondC (F7113) and Research Group 5 (FG5), from the AFOSR via PhoQuGraph (FA8655-20-1-7030) and QTRUST (FA9550-21- 1-0355), from the John Templeton Foundation via the Quantum Information Structure of Spacetime (QISS) project (ID 61466), and from the Austrian Federal Ministry for Digital and Economic Affairs, the National Foundation for Research, Technology and Development and the Christian Doppler Research Association. T. S. thanks Francesco Massa for helpful discussions.

*Corresponding author.
teodor.stroemberg@univie.ac.at
†Corresponding author.
philip.walther@univie.ac.at

[1] G. Chiribella, G. M. D'Ariano, P. Perinotti, and B. Valiron, Quantum computations without definite causal structure, Phys. Rev. A **88**, 022318 (2013).
[2] T. Colnaghi, G. M. D'Ariano, S. Facchini, and P. Perinotti, Quantum computation with programmable connections between gates, Phys. Lett. A **376**, 2940 (2012).
[3] G. Chiribella, Perfect discrimination of no-signalling channels via quantum superposition of causal structures, Phys. Rev. A **86**, 040301(R) (2012).
[4] A. Feix, M. Araújo, and Č. Brukner, Quantum superposition of the order of parties as a communication resource, Phys. Rev. A **92**, 052326 (2015).
[5] X. Zhao, Y. Yang, and G. Chiribella, Quantum Metrology with Indefinite Causal Order, Phys. Rev. Lett. **124**, 190503 (2020).
[6] L. M. Procopio, A. Moqanaki, M. Araújo, F. Costa, I. Alonso Calafell, E. G. Dowd, D. R. Hamel, L. A. Rozema, Č. Brukner, and P. Walther, Experimental superposition of orders of quantum gates, Nat. Commun. **6**, 7913 (2015).
[7] G. Rubino, L. A. Rozema, A. Feix, M. Araújo, J. M. Zeuner, L. M. Procopio, Č. Brukner, and P. Walther, Experimental verification of an indefinite causal order, Sci. Adv. **3**, e1602589 (2017).
[8] K. Goswami, C. Giarmatzi, M. Kewming, F. Costa, C. Branciard, J. Romero, and A. G. White, Indefinite Causal Order in a Quantum Switch, Phys. Rev. Lett. **121**, 090503 (2018).
[9] G. Rubino, L. A. Rozema, F. Massa, M. Araújo, M. Zych, Č. Brukner, and P. Walther, Experimental entanglement of temporal order, Quantum **6**, 621 (2022).

[10] K. Goswami, Y. Cao, G. A. Paz-Silva, J. Romero, and A. G. White, Increasing communication capacity via superposition of order, Phys. Rev. Res. **2**, 033292 (2020).
[11] G. Rubino, L. A. Rozema, D. Ebler, H. Kristjánsson, S. Salek, P. Allard Guérin, Č. Brukner, A. A. Abbott, C. Branciard, G. Chiribella, and P. Walther, Experimental quantum communication enhancement by superposing trajectories, Phys. Rev. Res. **3**, 013093 (2021).
[12] Y. Guo, X.-M. Hu, Z.-B. Hou, H. Cao, J.-M. Cui, B.-H. Liu, Y.-F. Huang, C.-F. Li, G.-C. Guo, and G. Chiribella, Experimental Transmission of Quantum Information Using a Superposition of Causal Orders, Phys. Rev. Lett. **124**, 030502 (2020).
[13] H. Cao, J. Bavaresco, N.-N. Wang, L. A. Rozema, C. Zhang, Y.-F. Huang, B.-H. Liu, C.-F. Li, G.-C. Guo, and P. Walther, Semi-device-independent certification of indefinite causal order in a photonic quantum switch, Optica **10**, 561 (2023).
[14] O. Oreshkov, F. Costa, and Č. Brukner, Quantum correlations with no causal order, Nat. Commun. **3**, 1092 (2012).
[15] M. Araújo, F. Costa, and Č. Brukner, Computational Advantage from Quantum-Controlled Ordering of Gates, Phys. Rev. Lett. **113**, 250402 (2014).
[16] M. J. Renner and Č. Brukner, Computational Advantage from a Quantum Superposition of Qubit Gate Orders, Phys. Rev. Lett. **128**, 230503 (2022).
[17] K. Wei, N. Tischler, S.-R. Zhao, Y.-H. Li, J. M. Arrazola, Y. Liu, W. Zhang, H. Li, L. You, Z. Wang, Y.-A. Chen, B. C. Sanders, Q. Zhang, G. J. Pryde, F. Xu, and J.-W. Pan, Experimental Quantum Switching for Exponentially Superior Quantum Communication Complexity, Phys. Rev. Lett. **122**, 120504 (2019).
[18] R. Simon and N. Mukunda, Minimal three-component SU(2) gadget for polarization optics, Phys. Lett. A **143**, 165 (1990).
[19] T. Strömberg, P. Schiansky, M. T. Quintino, M. Antesberger, L. Rozema, I. Agresti, Č. Brukner, and P. Walther, Experimental superposition of time directions, arXiv:2211.01283.
[20] P. Schiansky, T. Strömberg, D. Trillo, V. Saggio, B. Dive, M. Navascués, and P. Walther, Demonstration of universal time-reversal for qubit processes, Optica **10**, 200 (2023).
[21] V. S. Asadchy, M. S. Mirmoosa, A. Diaz-Rubio, S. Fan, and S. A. Tretyakov, Tutorial on electromagnetic nonreciprocity and its origins, Proc. IEEE **108**, 1684 (2020).
[22] M. Martinelli, A universal compensator for polarization changes induced by birefringence on a retracing beam, Opt. Commun. **72**, 341 (1989).
[23] B. E. Saleh and M. C. Teich, *Fundamentals of Photonics* (John Wiley & Sons, New York, 2019).
[24] See Supplemental Material at http://link.aps.org/supplemental/10.1103/PhysRevLett.131.060803 for technical details, universality proof and characterisation data.
[25] M. T. Quintino, https://github.com/mtcq (2022).
[26] J. Bavaresco, M. Murao, and M. T. Quintino, Strict Hierarchy between Parallel, Sequential, and Indefinite-Causal-Order Strategies for Channel Discrimination, Phys. Rev. Lett. **127**, 200504 (2021).
[27] C. Greganti, P. Schiansky, I. A. Calafell, L. M. Procopio, L. A. Rozema, and P. Walther, Tuning single-photon sources for telecom multi-photon experiments, Opt. Express **26**, 3286 (2018).
[28] J. Flórez, N. J. Carlson, C. H. Nacke, L. Giner, and J. S. Lundeen, A variable partially polarizing beam splitter, Rev. Sci. Instrum. **89**, 023108 (2018).
[29] P. Kurzyński and A. Wójcik, Quantum Walk as a Generalized Measuring Device, Phys. Rev. Lett. **110**, 200404 (2013).
[30] T. Strömberg *et al.*, Data for Demonstration of a Quantum Switch in a Sagnac Configuration (2023), 10.5281/zenodo.8171117.